ELEVATED REGION AREA MEASUREMENT FOR QUANTITATIVE ANALYSIS OF LASER BEAM MELTING PROCESS STABILITY

J. zur Jacobsmühlen[1], S. Kleszczynski[2], G. Witt[2], and D. Merhof[1]

[1]Institute of Imaging & Computer Vision, RWTH Aachen University, Germany
[2]Institute of Product Engineering, University of Duisburg-Essen, Germany

Abstract

Laser beam melting (LBM) processes enable layer-based production of geometrically complex metallic parts with very good mechanical properties for Rapid Manufacturing. Collisions between powder coating mechanism and elevated part regions pose a major risk to process stability, which is crucial for industrial application. Minimizing elevated region area usually involves parameter tuning in a trial-and-error approach, as the process outcome is the only measure of stability. One published approach to quantifying elevated region area utilizes an imaging system, which acquires layer images of the powder bed after powder deposition and detects elevated regions using image analysis. We extend the image-based analysis to each part region, create quantitative visualizations of elevated region area for quick assessment/comparison and compute a figure of merit. In experimental build jobs with overhanging structures and different support junction parameters we gain insight into problematic part regions, which can be used as feedback in job design. The presented method helps to improve LBM process stability, which is strongly linked to process efficiency.

Introduction

In laser beam melting processes, parts are built in a powder bed by selectively melting the current powder layer according to the part geometry. After lowering the build platform a recoater blade or roller moves powder from the powder container onto the build platform (Figure 1a) before the laser melts the next layer. All steps are repeated to build the entire part.

The possibility to produce complex and individual parts in a tool-less manufacturing process on the basis of CAD data was identified as the main driver of innovation in [1]. For industrial applications laser beam melting (LBM) is of special interest, due to the possibility to produce complex metal components with suitable mechanical properties. First LBM production lines are already established in the sector of medical technologies [2] and aerospace [3].

A problematic effect during LBM build jobs is the buildup of elevations, which stand out from the part layer (Figure 1b). As the powder layer is very thin (20 to 100 µm) these elevations are not covered by metal powder and may collide with the recoater blade causing
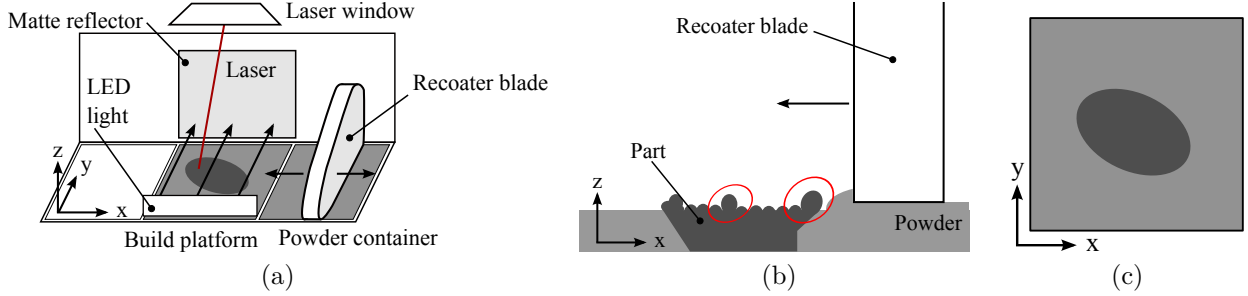
Figure 1: (a) The process chamber with the build platform and the recoater blade, (b) elevated part regions (highlighted) cause collisions between recoater blade and part, damaging either one or even both. (c) Example of acquired layer image.

damage to either one or even both. Severe elevations may cause process breakdowns by blocking the recoater blade, or destruction of thin parts, which are disrupted by the passing blade.

Consequently, the goal during the LBM job design phase is to minimize elevations in order to maximize process stability, which is required for reliable part production. Process monitoring and quantitative evaluation of elevations is needed to achieve this goal.

Several approaches to stability evaluation of LBM processes have been published. Reinarz and Witt [4] measured accelerations caused by contacts between blade and part by means of an accelerometer on the recoater blade. They defined thresholds for acceleration and interrupt the process when these are exceeded.

Krauss and Zäh [5] investigated the process reliability by building thin wall structures at different angles with respect to the coating blade and manually analyzing an image of the powder bed after deposition of a new powder layer. They observed collisions between part and recoater blade, which lead to mechanical distortions for thin (250 µm) wall structures.

Kruth et al. [6] developed an in-axis imaging system for melt pool monitoring and process control, which measures the size of the melt pool area. For overhanging structures the melt pool size increases due to the lower conductivity of metallic powder materials. This leads to melt process instabilities e.g. balling and overheating and consequently shape deviations and elevated part regions, which endanger process quality and stability. The developed system is able to detect changes of the melt pool size and adapts the laser power to keep it constant. This system is extended by mapping the acquired images to layer images and detecting process failures in [7]. The analysis of the mapped melt pool signal is applied to the layer before and the overhang layer itself to measure overheating for varying numbers of support structures.

We have presented an approach for the inspection and assessment of process stability in [8]. Here, an imaging system for acquisition of powder bed layer images [9] is used to evaluate the processing behavior for the support transition and overhanging structures by measuring total elevated region area and mean area of connected regions. The image-based measurements were validated against one-dimensional accelerometer measurements and showed good correlation.

Compared to the one-dimensional accelerometer measurements, two-dimensional measurements from powder bed layer images provide spatial information about elevations, which

helps to identify the probable cause, e.g. a critical geometrical feature. In this publication we extend the analysis of elevations detected in powder bed layer images by using imported reference part geometries and creating quantitative visualizations of elevations for all layers of a build job.

Method

We use an externally mounted monochrome CCD camera (29 Mpixels) with a tilt and shift lens to acquire layer images I_z of the powder bed before laser exposure. The image resolution ranges from 20 to 30 µm/pixel depending on the field of view (approx. 150 mm × 110 mm). Indirect lighting of the powder bed is provided by an LED line light at the machine front and a matte reflector at the machine back ([9], Figure 1a). It helps to reduce glare and reflections on the metallic part regions.

Image acquisition is triggered by the limit switches of the recoater blade to obtain layer images of the powder bed. There is one powder bed image $P_z \in \mathbb{Z}^{M \times N}$ for every layer in the build job, the index indicates the dependency on the layer's z position.

The detection method from [9] is based on the assumption that most pixels inside a powder bed image P_z show powder. We identify the image intensity as $I_z(x, y)$ with $(x, y) \in P_z$ and compute the intensity mean

$$\overline{I_z} = \frac{1}{MN} \sum_{x,y \in P_z} I_z(x, y),\tag{1}$$

which represents the powder. Then, elevations can be detected as outliers using a detection threshold

$$T_z = 3 \cdot \sigma,\tag{2}$$

where σ is the standard deviation of all pixel intensities $I_z(x, y)$ and the factor was determined experimentally. T_z is computed for every layer and the detection result is obtained as a binary mask image

$$D_z(x, y) = \begin{cases} 0 & I_z(x, y) \leq T_z \\ 1 & T_z < I_z(x, y) \end{cases},\tag{3}$$

The stride in z direction depends on the layer height, which is a process parameter and may range from 20 to 100 µm. Typical layer heights in our jobs are 40 µm for support structures and 20 µm for part layers.

As the recoater blade moves in x direction, large elevated areas at a single position x_0 are critical for the process stability as they are hit at the same time. Since we want to quantify the process stability we extract the elevated area $A_z(x)$ at every x position inside every layer image from the detection mask D_z as

$$A_z(x) = A_{\text{pixel}} \cdot \sum_{0 \leq y < M} D_z(x, y),\tag{4}$$

where A_{pixel} is the area of one pixel in mm^2. Figure 2 illustrates the measurement of elevated region area from powder bed images. A threshold for critical elevated area per x position was defined as $A_{\text{critical}} = 0.1\,\text{mm}^2$ based on accelerometer measurements [8].
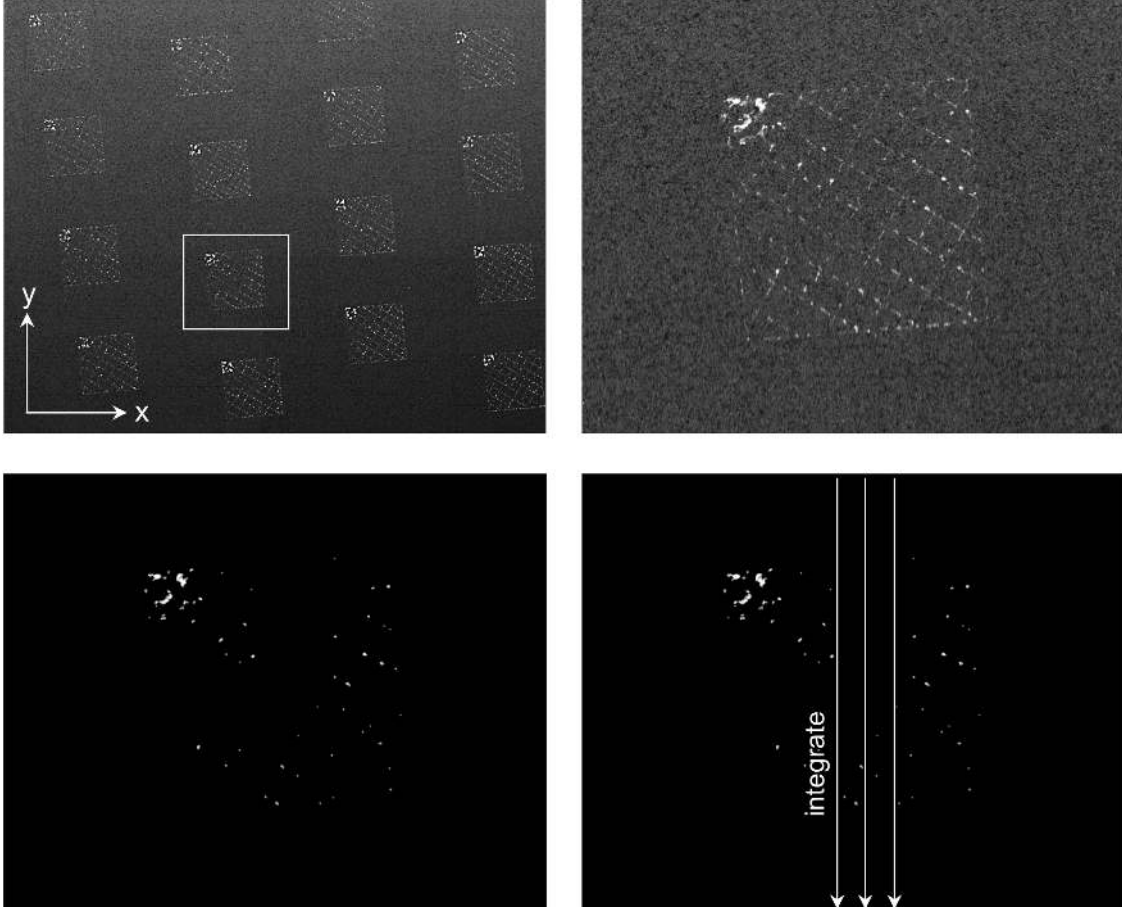
Figure 2: Example of elevated region segmentation and analysis. Top left: input powder bed layer image with visible elevated regions and highlighted region (scaled from 29 Mpixel). Top right: close-up of elevations of a single part with support structures. Bottom left: segmentation result based on method from [9] note that regions which are smaller than the laser focus diameter are excluded. Bottom right: integration of elevated regions to obtain $A_z(x)$ as a measure of elevation severity at every position x_0.

Overhanging regions in general and the down-skin in particular are the sections of the build job with the most elevations. Here, we are not only interested in the accumulated area at every position x_i but also in the region statistics, i.e. the spatial distribution. We analyze regions inside D_z using connected component analysis and compute their area $A_{R,z,i}$, and the total number of elevated regions N_R. For connected component analysis the implementation from [10] is used.

The described measurements can be carried out on entire layers, part regions (defined by their bounding boxes) and parts (defined by their geometry in each layer), see Figure 3. We import the part geometry from Common Layer Interface (CLI) files and store them along with the acquired layer images using the Hierarchical Data Format (HDF5). The analysis of part regions enables the separate analysis of multiple parts in a build job e.g. to compare process stability of identical parts built in a grid with varied process parameters.

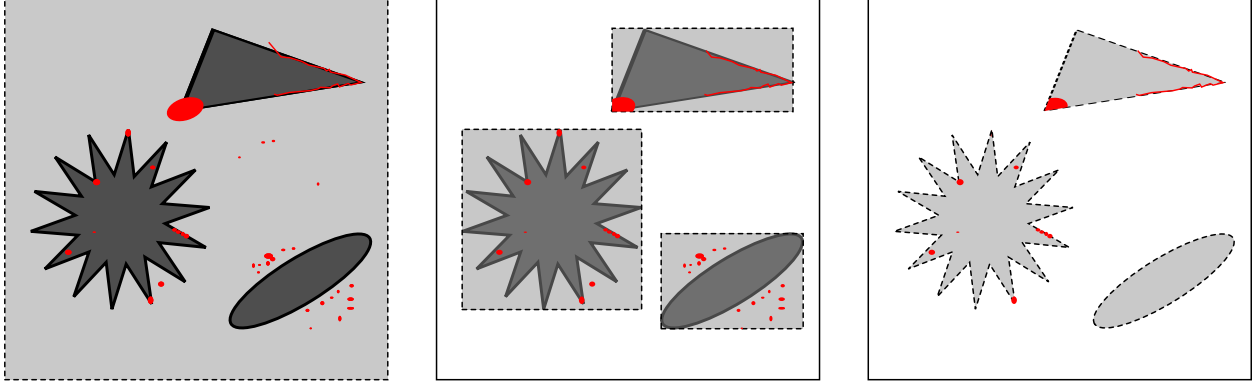For parts with support structures in part layers the analysis of part *regions* does not

Figure 3: Regions for elevation detection analysis (enclosed by dashed lines, elevations are shown in red). Left: entire layer, all elevations are taken into account, center: part regions defined by part bounding boxes, right: part area only, all elevations outside of part area are ignored.

differentiate between part and support structures which is undesirable e.g. if we want to analyze the influence of different support structure junction parameters. Here, the analysis of *parts* can be used to analyze these areas separately (Figure 3, right).

The availability of part geometries enables computing the relative elevated part area:

$$A_{\text{rel}}(x) = \begin{cases} \frac{A_z(x)}{A_{\text{part}}(x)} & \text{if } A_{\text{part}}(x) > 0 \\ 0 & \text{else,} \end{cases}, x \in [x_{\text{part,min}}, x_{\text{part,max}}] \tag{5}$$

which can be averaged over the entire part region $[x_{\text{part,min}}, x_{\text{part,max}}]$ and all L layers of a build job to obtain a single value for part comparison:

$$A_{\text{rel,avg}} = \frac{1}{L} \sum_x A_{\text{rel}}(x) \tag{6}$$

Quantitative visualization of elevated area for an entire part and all layers of a build job is complicated in a 3D visualization as the results of multiple layers would overlap, making it hard to see e.g. regions with increased elevated area. Instead, we propose to combine all elevated regions at specific positions x_i by integrating over y

$$A(x, z) = \sum_y D_z(x, y), \tag{7}$$

which yields cumulative vertical cross sections (x/z-plots) with color-coded elevated area. These plots enable identification of critical layers and localization of critical geometrical part features (Figure 5), and quick comparison of process stability for identical parts built with different parameters (Figure 7). A similar visualization was used in [11] for thermograms to identify hot spots.

For manual qualitative inspection of detected elevations of an entire build job a 3D visualization can be useful. We use ImageVis3D [12, 13] to visualize exported elevation layer image stacks (Figure 4).
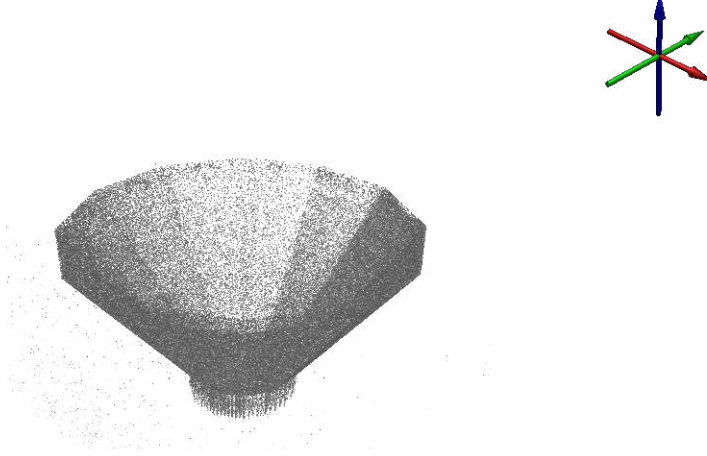
Figure 4: 3D visualization of elevations created from image stack using ImageVis3D [13]

Experimental Results

For build jobs with critical geometrical features the process design has to maximize the process stability. Overhanging geometries for instance are geometrical features with an increased risk of elevations. Using layer image analysis the critical overhang angle and the location of starting elevations can be identified and counter-measures can be taken, e.g. rotating the part to align with the movement of the powder blade. The optimum rotation angle has to be identified in experimental builds, which yield only a binary result: success or breakdown. Elevation analysis provides additional insight into the development of elevations during the build job and helps finding the transition from stable build to unstable build more precisely.

To evaluate our analysis methods we build two jobs on an EOSINT M 270 LBM system by EOS, Germany, using Hastelloy X:

- *job A*: 16 identical parts with overhanging geometries (Figure 5a), and

- *job B*: 25 cubes,

for which the support structures (number and size of teeth) were varied. For the cubes the starting layers were positioned at different z positions to avoid simultaneous interaction of multiple parts with the recoater blade.

Figure 5 shows the analysis results for the part area of a single part from job A. The plot of $A(x, z)$ shows larger elevations during the down-skin phase, $2.06\,\mathrm{mm} \leq z \leq 2.16\,\mathrm{mm}$, and for increasing polar angle of the overhang (measured with respect to the vertical) in higher layers, $z > 8.5\,\mathrm{mm}$ (Figure 5b). Most elevations are located at the part's boundaries and not inside. Critical elevations appear only at the right edge and for large polar angle.

These observations are supported by the elevation plots over z in Figure 5c, which show an initial bump at $z = 2.0\,\mathrm{mm}$ (yellow circle) and a gradual increase for $z > 8.2\,\mathrm{mm}$. For $z > 9.6\,\mathrm{mm}$ some layers are highlighted as $A_z(x)$ exceeds A_{critical} for some x positions (red triangles).
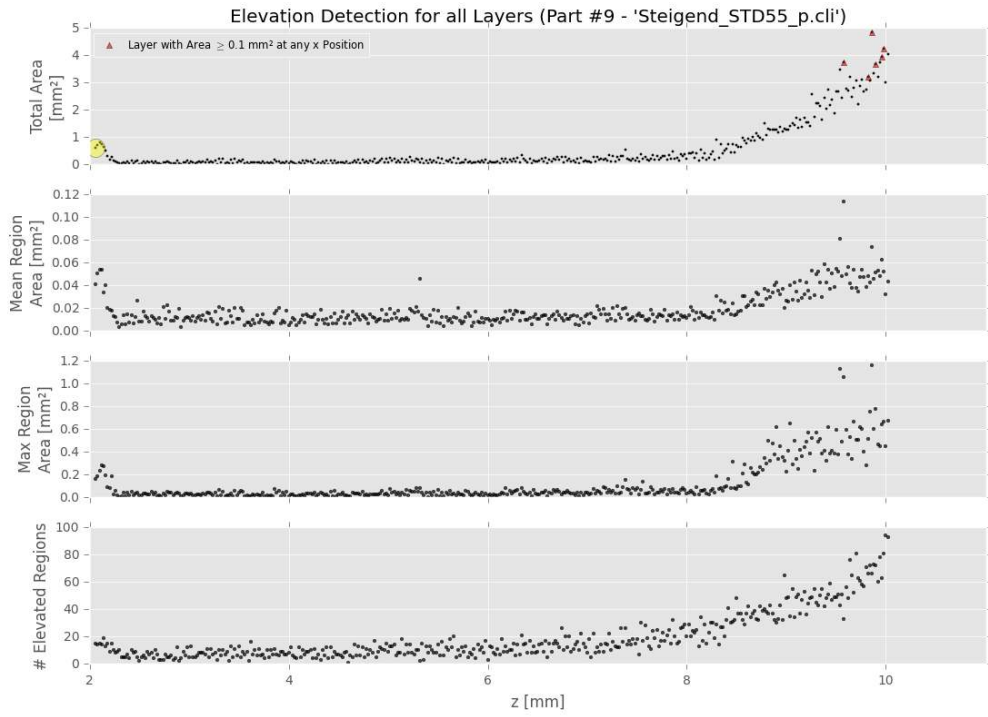
To evaluate the impact of different support structures in job B we analyze the part *regions* for three cubes in Figure 6. Support structures for parts STD35, STD36 and STD38 were
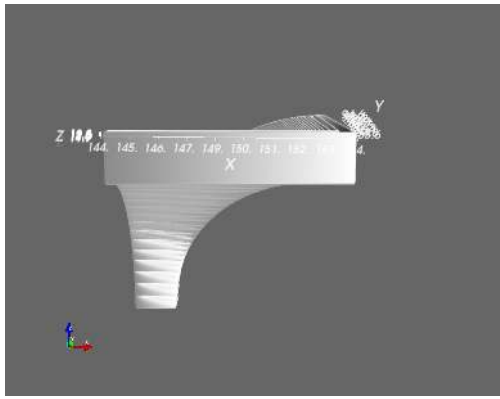
(a)
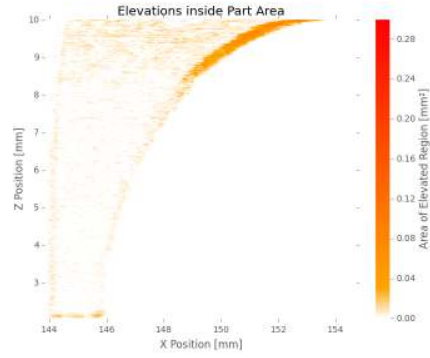
(b)

(c)

Figure 5: Analysis of overhanging geometry in x/z plot of elevated area. (a) part geometry with decreasing overhang angle for increasing z. (b) x/z plot of elevated area $A(x, z)$, the starting z position and thereby the overhang angle of increasing elevations can be identified by analyzing the right part boundary. (c) the elevation statistics show the buildup of elevations for increasing z position. Note that the build job was aborted before the rectangular top part was built.
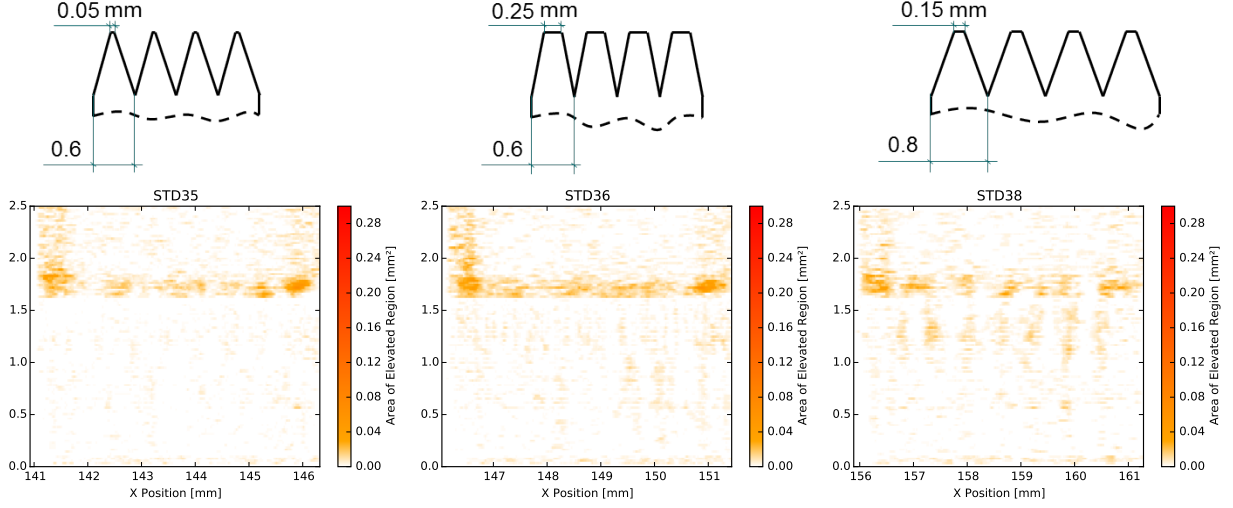
Figure 6: Analysis of different support structure configurations. Top: support configurations for connection to first part layer. Bottom: elevations in the part region (as defined by the part bounding box) for cubes from job B. Note that plots are cropped to $z \leq 2.5\,\mathrm{mm}$ to focus on the support structures.

built with identical teeth height of 0.9, different base length (0.6, 0.6 and 0.8) and varying top length (0.05, 0.25 and 0.15). The x/z plot shows almost no elevations in the support structures ($z < 1.6\,\mathrm{mm}$) for STD35, some elevations for STD36 and stronger elevations for STD38. Additionally, elevations in the first part layers ($z \approx 1.7\,\mathrm{mm}$) of STD35 and STD38 show a similar pattern, which is related to the regular structure of the supports. For STD36 the elevations are contiguous with two accumulation at the part corners. In conclusion, the configuration of STD35 achieves the highest process stability, while STD38 shows some critical elevations in the support structures, which may hinder usage in a batch job with multiple identical parts at the same x position.

Two identical geometries from job B, which start at different z positions are compared in Figure 7. Note that the plots of the part area start at the first part layer, whose z position depends on the part placement inside the build job. The integrated x/z plots show more elevations in the down-skin layers (bottom) of the right part and an accumulation of elevated regions at the left part boundary for both parts.

Additionally the relative elevated area $A_{\mathrm{rel}}(x)$ was computed for each part and used to rank the parts according to their mean relative elevated area $A_{\mathrm{rel,avg}}$ (Figure 8). This enables quick assessment of a part's process stability and can be used as a figure of merit during the job design phase.

Discussion

The color-coding of presented x/z plots is based on the critical area threshold $A_{\mathrm{critical}} = 0.1\,\mathrm{mm}^2$ defined in [8], where A_{critical} was linked to an acceleration of the recoater blade of $9\,\mathrm{m\,s}^{-2}$, and uses a gradient color from white to orange for $A(x,z) \leq A_{\mathrm{critical}}$ and from orange to red for $A_{\mathrm{critical}} < A(x,z) \leq 3 \cdot A_{\mathrm{critical}}$. This coding was selected experimentally to
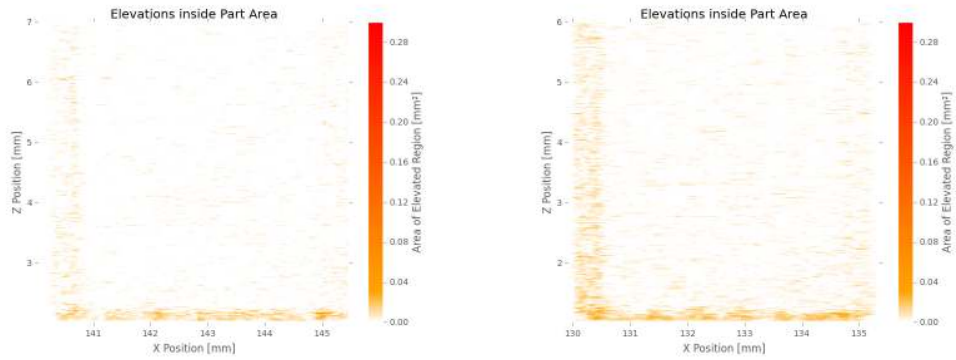
Figure 7: Analysis of elevations inside the part for two identical geometries positioned at different z positions.
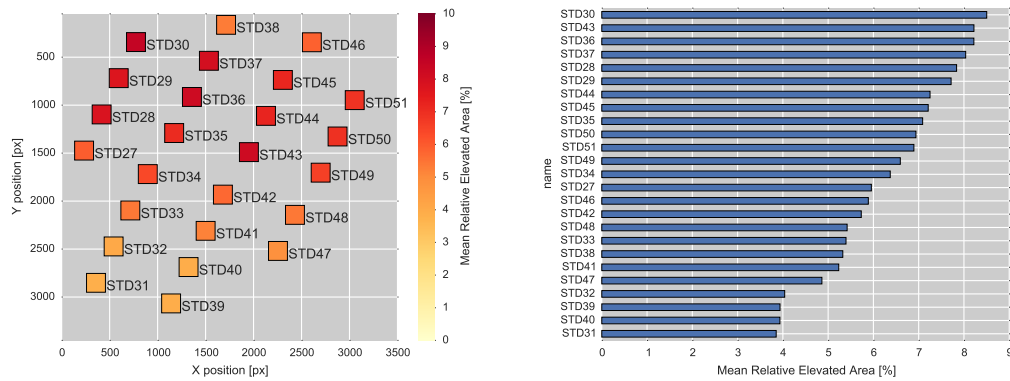

Figure 8: Relative elevated area plot. Analysis results for 25 identical cubes with different support parameters from a single build job. Part regions are colored according to their mean relative elevated area $A_{\mathrm{rel,avg}}$, which enables quick assessment and comparison of process stability for single parts. Displayed labels are part names.

visualize the differences in our build jobs and is not based on a comprehensive validation. Developing a validated color-coding could help to compare build job performance globally and avoid false alarms for stable jobs.

While the ranking of parts based on mean relative elevated area establishes a definite order, the observed values are very low and the applied color scale could exaggerate the differences between parts (Figure 8). An experimental validation and definition of boundaries for expected values under stable and unstable conditions will be performed in future work in order to provide recommendations for job stability optimization.

Conclusion

Elevations of part regions pose a major risk to build reliability of laser beam melting (LBM) processes as collisions between recoater blade and part may occur. Based on an image-based elevation detection method, we have presented quantitative measurement methods for analyzing part regions and parts for all layers of a build job. Visualization of elevated area $A(x, z)$ over x (direction of the recoater blade) and z (layer position) enables quick comparison of stability for different parts and localization of critical part regions, e.g. problematic geometrical features. Averaging the elevated area over all layers yields a single figure of merit, which can be used to rank part stability and identify optimum parameters (support structure, process parameter, part placement) with respect to process stability.

Our future work will focus on identifying and validating boundaries for the developed measures to provide a guideline in the build design phase.

References

[1] I. Gibson, D. W. Rosen, and B. Stucker, Additive Manufacturing Technologies – Rapid Prototyping to Direct Digital Manufacturing. Springer, 2010, ISBN: 978-1-4419-1119-3.

[2] H. Radovan, Z. Jozef, G. Bruno, L. Martin, , M. Lukas, J. Andrej, K. Rastislova, G. Miroslav, and L. Pasteur, "Additive Manufacturin, Verification and Implantation of Custom Titanium Implants – Case Studies," in Proceedings of 5th International Conference on Additive Technologies iCAT, 2014.

[3] J. Bamberg, K.-H. Dusel, and W. Satzger, "Overview of additive manufacturing activities at MTU aero engines," AIP Conference Proceedings, vol. 1650, no. 1, pp. 156–163, 2015. [Online]. Available: http://scitation.aip.org/content/aip/proceeding/aipcp/10.1063/1.4914605

[4] B. Reinarz and G. Witt, "Process Monitoring in the Laser Beam Melting Process - Reduction of Process Breakdowns and Defective Parts," in Proceedings of Materials Science & Technology 2012, 2012.

[5] H. Krauss and M. Zaeh, "Investigations on Manufacturability and Process Reliability of Selective Laser Melting," Physics Procedia, vol. 41, no. 0, pp. 815 – 822, 2013, lasers in Manufacturing (LiM 2013). [Online]. Available: http://www.sciencedirect.com/science/article/pii/S1875389213001673

[6] J.-P. Kruth, P. Mercelis, J. Van Vaerenbergh, and T. Craeghs, "Feedback control of selective laser melting," in Proceedings of the 3rd International Conference on Advanced Research in Virtual and Rapid Prototyping, September 2007, pp. 521–527.

[7] T. Craeghs, S. Clijsters, J.-P. Kruth, F. Bechmann, and M.-C. Ebert, "Detection of Process Failures in Layerwise Laser Melting with Optical Process Monitoring," Physics Procedia, vol. 39, no. 0, pp. 753 – 759, 2012. [Online]. Available: http://www.sciencedirect.com/science/article/pii/S1875389212026247

[8] S. Kleszczynski, J. zur Jacobsmühlen, B. Reinarz, J. T. Sehrt, G. Witt, and D. Merhof, "Improving Process Stability of Laser Beam Melting Systems," in Proceedings of the Fraunhofer Direct Digital Manufacturing Conference, A. Demmer, Ed., 2014.

[9] J. zur Jacobsmühlen, S. Kleszczynski, D. Schneider, and G. Witt, "High resolution imaging for inspection of Laser Beam Melting systems," in IEEE International Instrumentation and Measurement Technology Conference (I2MTC) 2013, 2013, pp. 707–712.

[10] S. van der Walt, J. L. Schönberger, J. Nunez-Iglesias, F. Boulogne, J. D. Warner, N. Yager, E. Gouillart, and T. Yu, "scikit-image: image processing in Python," PeerJ, vol. 2, p. e453, 6 2014. [Online]. Available: http://dx.doi.org/10.7717/peerj.453

[11] H. Krauss, T. Zeugner, and M. F. Zaeh, "Layerwise Monitoring of the Selective Laser Melting Process by Thermography," Physics Procedia, vol. 56, no. 0, pp. 64 – 71, 2014, 8th International Conference on Laser Assisted Net Shape Engineering {LANE} 2014. [Online]. Available: http://www.sciencedirect.com/science/article/pii/S1875389214002429

[12] T. Fogal and J. Krüger, "Tuvok, an Architecture for Large Scale Volume Rendering," in Proceedings of the 15th International Workshop on Vision, Modeling, and Visualization, November 2010. [Online]. Available: http://www.sci.utah.edu/ tfogal/academic/tuvok/Fogal-Tuvok.pdf

[13] CIBC, 2015, ImageVis3D: An interactive visualization software system for large-scale volume data. Scientific Computing and Imaging Institute (SCI), Download from: http://www.imagevis3d.org.